Full-Band Simulations of Single-Particle Resonant Tunneling in Transition Metal Dichalcogenide-Based Interlayer Tunneling Field-Effect Transistors

Xian Wu, Xuehao Mou, Leonard F. Register, and Sanjay K. Banerjee
Department of Electrical and Computer Engineering and Microelectronics Research Center
The University of Texas at Austin, Austin, Texas, USA
xianwu@utexas.edu

***Abstract*—We model and simulate the resonant tunneling and I-V characteristics of Interlayer Tunneling Field-Effect Transistors (ITFETs) based on transition metal dichalcogenide monolayers, MoS_2 layers here, using quantum transport simulations with a full-band model. Gate-controllable resonant peaks are demonstrated and the short channel effects on resonance broadening are studied.**

Keywords—resonant tunneling; tunneling transistor; transition metal dichalcogenide; quantum transport

I. Introduction

The Interlayer Tunneling Field-Effect Transistor (ITFET) (originally referred to as a "Double Electron Layer Tunneling Transistor" in [1]) is an attractive, non-conventional device intended for high-speed electronic applications. Based on conduction band (CB)-to-CB or valence band (VB)-to-VB resonant tunneling [2] between two two-dimensional (2D) electron gases separated by a tunnel barrier, ITFETs show gate-tunable negative differential resistance (NDR) characteristics [3,4], which can be applied to digital logic circuits [5].

Adjacent semiconductor quantum wells were the initial host proposed in [1] to achieve resonant tunneling for ITFETs. Recently, such resonant tunneling between the natural near-perfect 2D graphene layers has been studied both in theory and experiments [6-8]. Furthermore, quasi-2D monolayers of the transition metal dichalcogenides (TMDs) composed of a layer of transition metal atoms (Mo, W, etc.) sandwiched by two layers of chalcogen atoms (S, Se, etc.) [9], also provide a promising platform for ITFETs. Use of TMDs may reduce short-channel resonance broadening associated Heisenberg uncertainty.

Due to the complex band structures, the modeling of TMD materials in electronic devices commonly employs simple effective-mass-based parabolic band approximations [10], which neglects their nonparabolicity and higher-lying energy bands. In this paper, we apply a more accurate multi-band model for, for specificity here, MoS_2 monolayers to study the resonant tunneling effect and I-V characteristics of short channel ITFETs based on these less explored materials.

II. Simulation Method

A. Device concept

Fig. 1(a) shows the structure of a MoS_2-based ITFET schematically, where two MoS_2 monolayers are partially overlapped with a tunnel barrier layer between. The left end of the top (T) MoS_2 layer and the right end of the bottom (B) MoS_2 layer extending beyond the overlap region serve as the electrical leads and are separately biased. In this paper, the bottom right or "source" (S) lead is always grounded and the top left or "drain" (D) lead is biased with voltage V_{DS}, which creates a Fermi level difference between two leads $E_{F,D}-E_{F,S}= -eV_{DS}$ where e is the magnitude of the electron charge. Electrons in the overlap region are controlled by a back gate with voltage V_{BG} and a top gate with voltage V_{TG}. It is possible for electrons or holes to tunnel from one layer to the other in this region, forming an interlayer tunneling current. The magnitude of the tunneling current depends on the alignment of the band structures in two layers and the Fermi level difference between them, as illustrated by Fig. 1(b). If carrier energies and in-plane crystal momenta are well defined, then when the band structures are aligned (when the difference $\Delta\varphi$ between the electrostatic potentials in the top layer (φ_T) and the bottom layer (φ_B) becomes zero) a non-zero V_{DS} can lead to a large resonant interlayer tunneling current, but when $\Delta\varphi$ is nonzero, energy and momentum cannot be conserved simultaneously and the current would be eliminated. However, in practice weaker but nonzero currents still can flow off-resonance due to energy or momentum uncertainty in the tunneling process, such as due to scattering and, as to be considered here, short channel effects.

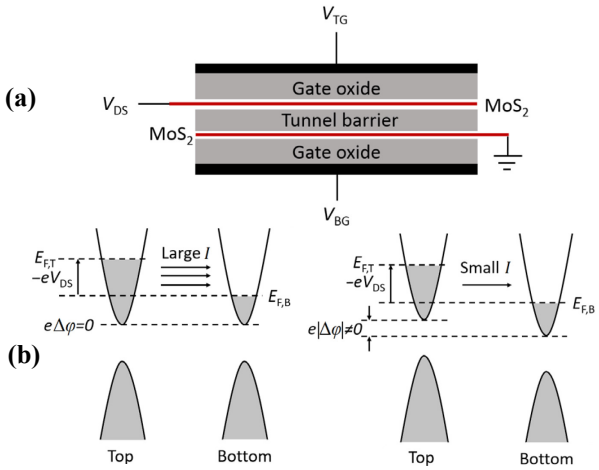

Fig. 1. (a) Schematic structure and biasing scheme of a MoS_2-based ITFET. (b) Band digrams illustrating the operation of ITFETs in (left panel) and out of (right panel) resonance. $\Delta\varphi$ is the electrostic potential difference between the layers, which is a function of souce (S), drain (D), and top (T) and bottom (B) gate voltages.

This work was supported by the Semiconductor Research Corporation's Nanoelectronics Research Initiative (SRC-NRI) via the South West Academy of Nanoelectronics (SWAN). Supercomputing resources were provided by the Texas Advanced Computing Center (TACC).

978-1-5090-0818-6/16/$31.00 ©2016 IEEE

B. Electrostics modeling

Rigorously, φ_{T} and φ_{B} are functions of position along the tunneling region and should be calculated self-consistently using the Poisson's equation along with the transport calculations discussed in the upcoming Section II-C. For the purpose of capturing the underlying principles of ITFETs here, we approximate φ_{T} and φ_{B}, as well as the Fermi levels $E_{\mathrm{F,T}} = E_{\mathrm{F,D}}$ and $E_{\mathrm{F,B}} = E_{\mathrm{F,S}}$, as uniform within the respective layers. Therefore, the quasi-one-dimensional capacitive relations give

$$\begin{aligned} e\left(p_{\mathrm{T}} - n_{\mathrm{T}} + N_{\mathrm{D,T}}^{(+)} - N_{\mathrm{A,T}}^{(-)}\right) &= C_{\mathrm{G,T}}\Delta\varphi_{\mathrm{OX,T}} + C_{\mathrm{I}}(\varphi_{\mathrm{T}} - \varphi_{\mathrm{B}}) \\ e\left(p_{\mathrm{B}} - n_{\mathrm{B}} + N_{\mathrm{D,B}}^{(+)} - N_{\mathrm{A,B}}^{(-)}\right) &= C_{\mathrm{G,B}}\Delta\varphi_{\mathrm{OX,B}} + C_{\mathrm{I}}(\varphi_{\mathrm{B}} - \varphi_{\mathrm{T}}) \end{aligned} \quad (1)$$

where n_{T} and p_{T} (n_{B} and p_{B}) are the electron and hole concentrations as functions of φ_{T} (φ_{B}) and the Fermi level $E_{\mathrm{F,T}}$ ($E_{\mathrm{F,B}}$) in the top (bottom) layer; $N_{\mathrm{D}}^{(+)}$ and $N_{\mathrm{A}}^{(-)}$ are the similarly defined ionized donor or acceptor concentrations; $C_{\mathrm{G,T}}$ ($C_{\mathrm{G,B}}$) is the top (bottom) gate oxide capacitance; C_{I} is the tunnel barrier capacitance; $\Delta\varphi_{\mathrm{OX,T}}$ ($\Delta\varphi_{\mathrm{OX,B}}$) is the electrostatic potential drop across the top (bottom) gate oxide determined by φ_{T} (φ_{B}), gate voltage V_{TG} (V_{BG}) and the gate material work function and electron affinity of the MoS_2 monolayer [10]. Thus, φ_{T} or φ_{B} are ultimately controlled by all four-terminal voltages.

Illustratively, here we use a capacitance equivalent to that of 1 nm SiO_2 for C_{I}, $C_{\mathrm{G,T}}$ and $C_{\mathrm{G,B}}$, ideal undoped channels, 4.3 eV effective electron affinity for MoS_2, and 4.1 eV work function for both gates. Under these conditions, the CB edge in each layer is located near the Fermi level under small voltages.

C. Tansport simulation approach

The bulk crystal structure of a MoS_2 monolayer has a hexagonal primitive lattice. In order to model the transport properties, we use a rectangular unit cell in the *x*-*y* plane with twice the area of a primitive unit cell, as shown in Fig. 2(a). The lattice vectors of this unit cell arrangement are $\mathbf{a}_x$ are $\mathbf{a}_y$. We take the direction of current flow to be along the *x* axis and number the unit cells as shown in Fig. (b). The n=1 and n=N cells are the left and right boundaries of the tunneling region, respectively.

To describe the electronic structure of the MoS_2 layers, here as in [11] we use a tight-binding model with a basis set of maximally-localized Wannier functions (MLWFs) [12] $|nm\alpha\rangle$ with hopping matrices $(\mathbf{H}_{nm,n'm'}^{(\mathrm{hop})})_{\alpha\alpha'} = \langle nm\alpha|\mathbf{H}|n'm'\alpha'\rangle$ calculated from density functional theory (DFT) using OpenMX [13]. Here $|nm\alpha\rangle$ denotes the αth basis function in the unit cell denoted by $n\mathbf{a}_x + m\mathbf{a}_y$. In this study we use the Mo atom's d_{z^2}, d_{xy} and $d_{x^2-y^2}$ orbitals, including separate spin up and down orbitals to allow for spin-splitting, from which to construct the MLWFs and obtain $M = 12$ basis functions in a bilayer rectangular unit cell. The electron states $|\psi\rangle$ in this system can be written as a linear combination of all oribtals $|nm\alpha\rangle$ with coefficients $\psi_{nm\alpha}$. We write $\boldsymbol{\psi}_{nm} = (\psi_{nm1}, \cdots, \psi_{nmM})^{\mathrm{T}}$ to denote the tight-binding wavefunction within each cell.

We treat our device as sufficiently wide so that translation invariance in *y* direction is retained and Bloch's theorem can be applied. For the state with wave-vector k_y in the *y* direction, $\boldsymbol{\psi}_{nm}(k_y) = e^{ik_y m a_y}\boldsymbol{\psi}_{n0}(k_y)$, we write $\boldsymbol{\psi}_n(k_y)$=$\boldsymbol{\psi}_{n0}(k_y)$ and $\mathbf{H}_{nn'}^{(\mathrm{hop})}(k_y) = \sum_m e^{ik_y m a_y}\mathbf{H}_{n0,n'm}^{(\mathrm{hop})}$. For the following analysis, k_y is included implicitly in $\boldsymbol{\psi}_n$, $\mathbf{H}_{nn'}^{(\mathrm{hop})}$ and related terms.

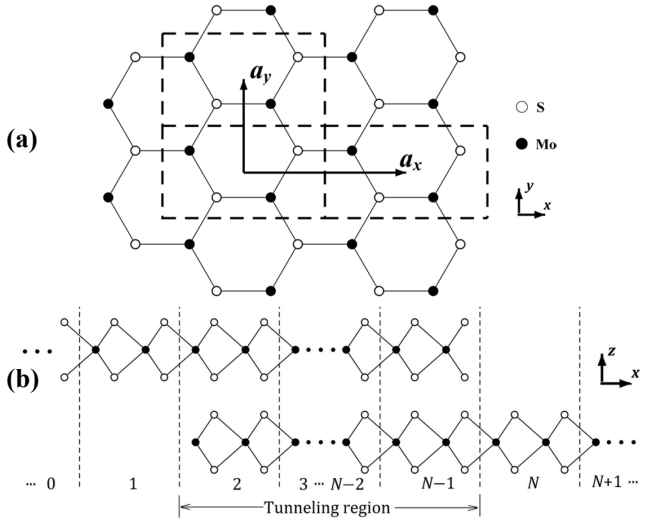

Fig. 2. Top (a) and side (b) views of the crystal structure of the MoS_2 monolayers in Fig. 1. We used a rectangular unit cell in the *x*-*y* plane and number the cells in the *x* direction. Tunneling occurs within the the tunneling region from n=2 cell to n=N-1 cell.

Similar to the work of [11], the Hamiltonian of this system has the form

$$\mathbf{H}_{nn'} = \begin{bmatrix} \mathbf{H}_{nn',\mathrm{T}}^{(\mathrm{hop})} - e\varphi_{\mathrm{T}}\mathbf{I} & \mathbf{H}_{\mathrm{n,T};n',\mathrm{B}} \\ \mathbf{H}_{\mathrm{n,B};n',\mathrm{T}} & \mathbf{H}_{nn',\mathrm{B}}^{(\mathrm{hop})} - e\varphi_{\mathrm{B}}\mathbf{I} \end{bmatrix}, \quad (2)$$

where $\mathbf{I}$ is the unitary matrix; $\mathbf{H}_{nn',\mathrm{T}}^{(\mathrm{hop})}$ and $\mathbf{H}_{nn',\mathrm{B}}^{(\mathrm{hop})}$ are the *intra*-layer tight-binding hopping matrices of each MoS_2 monolayer obtained from the DFT calculations; $\mathbf{H}_{\mathrm{n,T};n',\mathrm{B}}$ and $\mathbf{H}_{\mathrm{n,B};n',\mathrm{T}}$ describe the *inter*layer interactions. In this study we simply take $\mathbf{H}_{\mathrm{n,T};n',\mathrm{B}}$ and $\mathbf{H}_{\mathrm{n,B};n',\mathrm{T}}$ equal to $t\mathbf{I}$ when $1 < n = n' < N$ and equal to 0 otherwise, such that interlayer hopping occurs only between the same basis functions in nearest interlayer cells in the tunneling region. We then use the scalar parameter t to describe the interlayer tunnel strength. In further studies, these matrices can be replaced by more accurate hopping matrices through specific interlayer barriers from DFT calculations, or even by matrices including non-local interactions, e.g., the Fock exchange interaction as in [14].

In the transport direction, we assume that the leads are semi-infinite and perfectly absorbing. Thus, for each energy E and wave-vector k_y, the wavefunction of the ITFET in the leads ($n \le 1$ or $n \ge N$) can be written as $\boldsymbol{\psi}_n = \boldsymbol{\psi}_n^+ + \boldsymbol{\psi}_n^-$, where the plus (minus) signed term indicates the components propagating or evanescing in the positive (negative) *x* direction. In turn, $\boldsymbol{\psi}_n^+$ ($\boldsymbol{\psi}_n^-$) can be written as a linear combination of the multiple independent right (left) propagating or evanescing modes of these leads, $\boldsymbol{\phi}_i^+$ ($\boldsymbol{\phi}_i^-$), with complex phase factors λ_i^+ (λ_i^-),

$$\boldsymbol{\psi}_n^{\pm} = \textstyle\sum_i c_i^{\pm}(\lambda_i^{\pm})^n\boldsymbol{\phi}_i^{\pm}. \quad (3)$$

All of these lead modes can be obtained by solving the quadratic eigenvalue equations,

$$\mathbf{H}_{10}\boldsymbol{\phi} + \lambda\mathbf{H}_{00}\boldsymbol{\phi} + \lambda^2\mathbf{H}_{01}\boldsymbol{\phi} = \lambda E\boldsymbol{\phi}, \quad (4\text{-a})$$

$$\mathbf{H}_{N(N+1)}\boldsymbol{\phi} + \lambda\mathbf{H}_{(N+1)(N+1)}\boldsymbol{\phi} + \lambda^2\mathbf{H}_{(N+1)(N+2)}\boldsymbol{\phi} = \lambda E\boldsymbol{\phi}, \quad (4\text{-b})$$

considering nearest neighbor *rectangular* unit cells in the *x* direction (four or more nearest neighbor atomic planes) where (4-a) is for the D lead and (4-b) for the S lead. Each equation,

(4-a) and (4-b), has $2M$ non-zero solutions, where, again, M is the number of basis functions in a unit cell. M of these solutions, $\boldsymbol{\phi}_i^+$ and λ_i^+, are the modes that either propagate ($|\lambda_i^+| = 1$) or evanesce ($|\lambda_i^+| < 1$) in the positive x direction, with only the propagating modes carrying current. The remaining M solutions, $\boldsymbol{\phi}_i^-$ and λ_i^-, are the modes that either propagate ($|\lambda_i^-| = 1$) or evanesce ($|\lambda_i^-| > 1$) in the negative x direction.

Use of (3) and (4) allows us to relate the wave function components of an electron state of the ITFET system at two adjacent cells in the leads, e.g., $\boldsymbol{\psi}_1^+$ and $\boldsymbol{\psi}_0^+$ ($\boldsymbol{\psi}_1^-$ and $\boldsymbol{\psi}_0^-$), by

$$\boldsymbol{\psi}_1^{\pm} = \mathbf{T}_{\mathrm{D}\pm}\boldsymbol{\psi}_0^{\pm} = \mathbf{Q}_{\pm}\mathbf{P}_{\pm}\mathbf{Q}_{\pm}^{-1}\boldsymbol{\psi}_0^{\pm}, \tag{5}$$

where

$$\mathbf{Q}_{\pm} = \left(\boldsymbol{\phi}_1^{\pm}, \boldsymbol{\phi}_2^{\pm}, \cdots, \boldsymbol{\phi}_M^{\pm}\right),\ \mathbf{P}_{\pm} = \mathrm{diag}\left(\lambda_1^{\pm}, \lambda_2^{\pm}, \cdots, \lambda_M^{\pm}\right) \tag{6}$$

with $\boldsymbol{\phi}_i^{\pm}$ and $\lambda_i^{\pm}$ solved from (4-a). Similar relations can be obtained between $\boldsymbol{\psi}_{N+1}^{\pm}$ and $\boldsymbol{\psi}_N^{\pm}$ via $\mathbf{T}_{\mathrm{S}\pm}$ constructed using the solutions from (4-b).

With these relations, we can use the approach as in [14] to set up a transport equation for the channel region

$$(E\mathbf{I} - \mathbf{H} - \boldsymbol{\Sigma})\boldsymbol{\Psi} = \mathbf{S}, \tag{7}$$

where $\mathbf{H} = \left[\mathbf{H}_{ij}\right]_{NM\times NM}$, $\boldsymbol{\Sigma} = \left[\boldsymbol{\Sigma}_{ij}\right]_{NM\times NM}$, $\boldsymbol{\Psi} = [\boldsymbol{\psi}_i]_{NM\times 1}$, $\mathbf{S} = [\mathbf{s}_i]_{NM\times 1}$ with $i,j = 1,\cdots,N$, $\boldsymbol{\Sigma}_{11} = \mathbf{H}_{10}\mathbf{T}_{\mathrm{D}-}^{-1}$, $\mathbf{s}_1 = \mathbf{H}_{10}(\mathbf{I} - \mathbf{T}_{\mathrm{D}-}^{-1}\mathbf{T}_{\mathrm{D}+})\boldsymbol{\psi}_0^+$, $\boldsymbol{\Sigma}_{NN} = \mathbf{H}_{N(N+1)}\mathbf{T}_{\mathrm{S}+}$, $\mathbf{s}_N = \mathbf{H}_{N(N+1)}(\mathbf{I} - \mathbf{T}_{\mathrm{S}+}\mathbf{T}_{\mathrm{S}-}^{-1})\boldsymbol{\psi}_{N+1}^-$, and all remaining $\boldsymbol{\Sigma}_{i,j}$ and $\mathbf{s}_i$ are zero.

For any given energy E and k_y we first solve (4) to obtain all transport modes in each lead. Each propagating mode $\boldsymbol{\phi}_i^{\pm}$ with incident propagation direction injects into the channels, producing an associated $\boldsymbol{\psi}_0^{(+)}$ or $\boldsymbol{\psi}_{N+1}^{(-)}$ as required for the source term $\mathbf{S}$ in (7). With $\mathbf{S}$ the ITFET state $\boldsymbol{\Psi}$ for that incident lead mode be obtained from (7). The tight-binding probability current flow carried by this ITFET state $\boldsymbol{\Psi}$ is [15]

$$\begin{aligned} j_{e,\mathrm{D}}^{\pm} &= 2\,\mathrm{Im}\left(\boldsymbol{\psi}_1^{\pm\dagger}\mathbf{H}_{10}\boldsymbol{\psi}_0^{\pm}\right)/\hbar \\ j_{e,\mathrm{S}}^{\pm} &= 2\,\mathrm{Im}\left(\boldsymbol{\psi}_{N+1}^{\pm\dagger}\mathbf{H}_{(N+1)N}\boldsymbol{\psi}_N^{\pm}\right)/\hbar \end{aligned} \tag{10}$$

The total probability current flow is thus

$$j_e = j_{e,\mathrm{D}} = j_{e,\mathrm{S}} = j_{e,\mathrm{D(S)}}^{+} + j_{e,\mathrm{D(S)}}^{-} \tag{11}$$

The transmission coefficient T for the state injected into the D (S) lead can be defined as

$$T_{\mathrm{D(S)}} = j_{e,\mathrm{S(D)}}^{+(-)}/j_{e,\mathrm{D(S)}}^{+(-)} \tag{12}$$

Note that for any injection state labeled by energy E, wave vector k_y, injection lead i, and index n from solving (4), (7) can be set up and solved independently. Therefore parallelized computing is readily used to reduce computing time.

Finally, the total macroscopic charge current is

$$j_{\mathrm{DS}} = -e\sum_{E,k_y,i,n} f\left(E - E_{\mathrm{F},i}\right)j_e(E,k_y,i,n) \tag{13}$$

where $f(E)$ is the Fermi distribution function.

III. Results

Fig. 3 shows the transmission coefficient T of a randomly-chosen injection state near the CB edge as a function of the interlayer potential difference $\Delta\varphi$, with different channel lengths L and different hopping strengths t. As expected, this state has a strong transmission peak near $\Delta\varphi$=0 where resonant tunneling occurs. With a shorter channel, this peak is weakened and broadened, which is undesired and needs to be suppressed for the logic gates based on ITFETs [1]. This broadening is due to Heisenberg momentum-position uncertainty for the finite channel length, translated to energy uncertainty via the charge carrier incident group velocities $v = \partial E/\hbar\partial k$. Thus, slower carriers produce less broadening, turning the heavy mass carriers in TMDs into an advantage. A moderate interlayer hopping strength doesn't affect the shape of the transmission curves. However, a large t, e.g. 10 meV in Fig. 3(b), leads to the peak transmission probability saturating toward unity near $\Delta\varphi$=0. This saturation also effectively broadens the resonant tunneling by increasing the relative importance of the off-resonance tails which are not in saturation. Therefore, the tunneling barrier should be designed to allow sufficient tunneling current without excessively broadening the resonant tunneling.

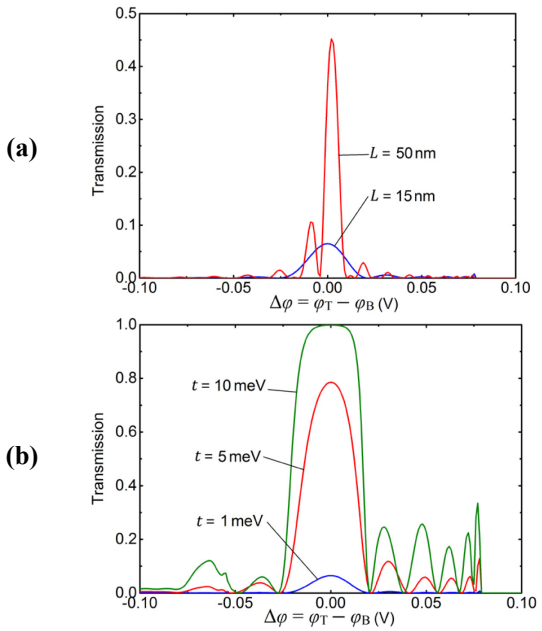

Fig. 3. Transmission probability of a single injection state as a function of channel potential difference with (a) different channel lengths and (b) different interlayer hopping strengths. Note saturation of the tunneling probability to unity for strong interlayer coupling in (b). In (a) the hopping parameter is t = 1 meV. In (b) the channel length is L = 15 nm.

The I-V curves in Fig. 5(a) present gate-controllable resonant tunneling in ITFETs for non-saturating and in saturating current. With the back gate grounded (V_{BG}=0), the channel potentials in two layers shift with respect to each other under different V_{TG}, which, in turn, leads to resonant tunneling at different V_{DS} providing the mechanism of gate control. With our simulation parameters, a 0.2 V V_{TG} is sufficient to shift the resonant V_{DS} by only 25 mV, but this change still should be sufficient for switching in bi-stable logic gates in [1] in the absence of current saturation.

The degree of off-resonance current in the I-V tails at positive V_{DS} and the asymmetries with respect to both V_{TG} and V_{DS} in Fig. 5(a) are associated with the filling of the channel states consistent with the density of states. This behavior can be effectively described via a quantum capacitance C_{Q} connected in series between the lead and channel [16]. As illustrated in Fig. 5(b), when a positive (negative) V_{TG} is applied, the Fermi level

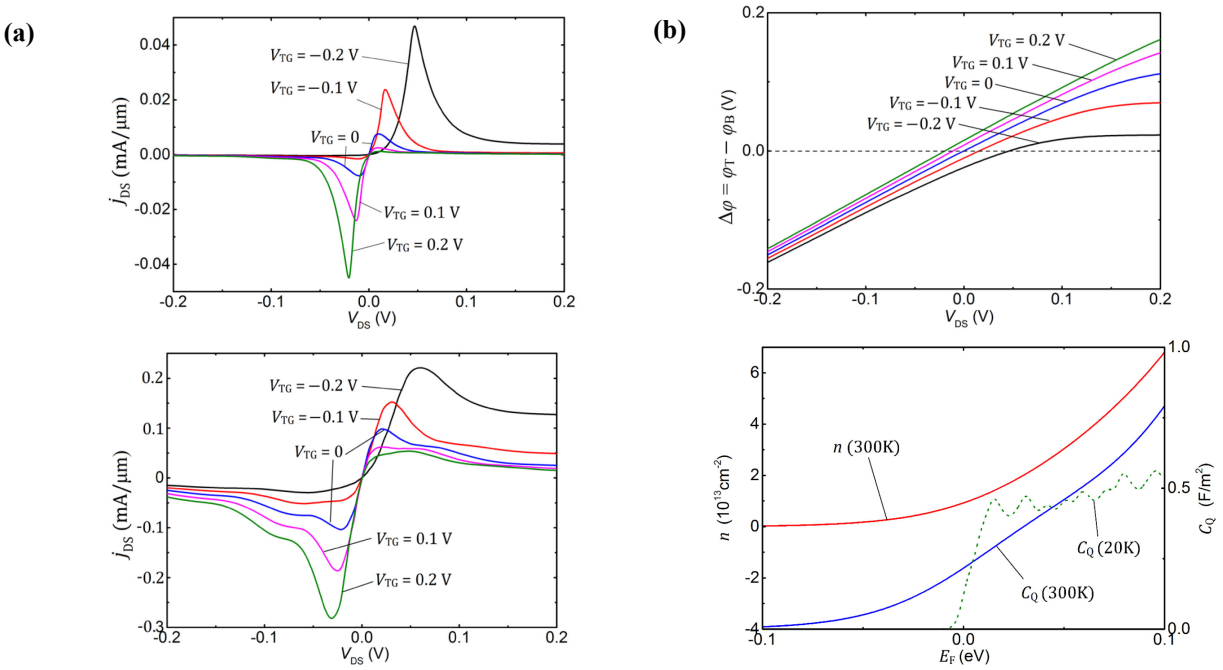

Fig. 5. (a) I-V characteristics of ITFETs at room temperature under different V_{TG} with t = 1 meV (top panel) and t = 10 meV (bottom panel). (b) Channel potential difference $\Delta\varphi$ as a function of V_{DS} (top panel) and electron concentration n and quantum capacitance C_Q as a function of Fermi level E_F relative to the CB edge (bottom panel) within these non-parabolic bands at room temperature. A positive V_{TG} drives E_F to larger C_Q regime, therefore $\Delta\varphi$ has an almost linear dependence on V_{DS}. However a negative V_{TG} reduces C_Q and leads to the weaker control of V_{DS} over $\Delta\varphi$. The 20K C_Q is shown for reference, displaying the the abrupt capacitance onset and near-constant value above onset expected within the parabolic regime. However, at 300K the thermal distribution smooths the onset and couples to the higher energy band structure producing the shown C_Q. All the above simulations were performed with 15 nm channel and V_{BG} = 0.

shifts to a higher (lower) C_Q regime and, thus, the drain has better (worse) control over the channel, while the gate has less (more) control. Note that the 300K thermal carrier distribution smoothes out the onset of capacitance with band filling, and also couples to the non-parabolic higher energy band structure increasing the C_Q. Because the location of the Fermi level in Fig. 5(b) are determined by the MoS_2 electron affinity, work function of the gates, and doping which is not discussed here, careful engineering of these parameters will be needed to maximize gate control.

IV. Conclusion

We demonstrate the theoretical feasibility of achieving gate-controllable resonant tunneling of an ITFET based on bilayer MoS_2 system. Tradeoffs of improving the ITFET performances are addressed. A sharp resonant peak is desired for ITFET-based logic gates. However, device scaling broadens the peak. A larger interlayer tunneling strength required for a sufficient current also broadens the resonance peak. Low resistivity is also desired for the MoS_2 layers to carry sufficient current, which requires higher carrier concentrations. However, as illustrated in Fig. 5, this will lead to a high C_Q, which weakens the gate control over the resonance.

In terms of the simulation method, we incorporated a multi-band model for MoS_2 monolayers into quantum transport simulations. Some of the underlying physics, e.g. the effect of quantum capacitances, can be addressed here more accurately than by a parabolic model. Furthermore, with the inclusion of non-local exchange effects, this method should allow consideration of current flow in the presence of possible interlayer exciton formation [14] in perhaps more compatible TMD systems, for exotic devices applications such as the Bilayer pseudoSpin Field-Effect Transistor (BiSFET) in [17].

References

[1] J. A. Simmons, M. A. Blount, J. S. Moon, W. E. Baca, J. L. Reno, and M. J. Hafich, *IEDM 1997*, 755 (1997)

[2] L. L. Chang, L. Esaki, and R. Tsu, *Appl. Phys. Lett.*, **24**, 593 (1974)

[3] B. Fallahazad, K. Lee, S. Kang, J. Xue, S. Larentis, C. Corbet *et al.*, *Nano Lett.*, **15**, 428 (2015)

[4] S. Kang, B. Fallahazad, K. Lee, H. Movva, K. Kim, C. M. Corbet *et al.*, *IEEE Elec. Dev. Lett.*, **36**, 405 (2015)

[5] P. Mazumder, S. Kulkarni, M. Bhattacharya, J. P. Sun, and G. I. Haddad, *Proceedings of the IEEE*, **86**, 664 (1998)

[6] L. Britnell, R. V. Gorbachev, A. K. Geim, L. A. Ponomarenko, A. Mishchenko, M. T. Greenaway *et al.*, *Nature Comm.*, **4**, 1794 (2013)

[7] D. Reddy, L. F. Register, and S. K. Banerjee, *DRC 2012*, 73 (2012)

[8] R. M. Feenstra, D. Jena, and G. Gu, *J. Appl. Phys.*, **111**, 043711 (2012)

[9] Q. H. Wang, K. Kalantar-Zadeh, A. Kis, J. N. Coleman, and M. S. Strano, *Nature Nanotech.*, **7**, 699 (2012)

[10] M. Li, D. Esseni, G. Snider, D. Jena, and H. G. Xing, *J. Appl. Phys.*, **115**, 074508 (2014)

[11] X. Wu, X. Mou, L. F. Register, and S. K. Banerjee, *SISPAD 2015*, 124 (2015)

[12] N. Marzari, A. A. Mostofi, J. R. Yates, I. Souza, and D. Vanderbilt, *Rev. Mod. Phys.*, **84**, 1419 (2012)

[13] T. Ozaki, http://www.openmx-square.org/

[14] X. Mou, L. F. Register, A. H. MacDonald, and S. K. Banerjee, *Phys. Rev. B*, **92**, 235413 (2015)

[15] T. N. Todorov, *J. Phys.: Condens. Matter*, **14**, 3049 (2002)

[16] S. Luryi, *Appl. Phys. Lett.*, **52**, 501 (1988)

[17] S. K. Banerjee, L. F. Register, E. Tutuc, D. Reddy, and A. H. MacDonald, *IEEE Elec. Dev. Lett.*, **30**, 158 (2009)